www.MaterialsViews.com

Sub-1 nm Nickel Molybdate Nanowires as Building Blocks of Flexible Paper and Electrochemical Catalyst for Water Oxidation

*Huiling Liu, Haoyi Li, Peilei He, and Xun Wang**

To promote the development of nanotechnology, a key challenge is to construct novel nanostructures through effective synthetic methods, and these two aspects always impact each other. Ultrathin nanocrystals as a recently appeared structure have been demonstrated to possess superior properties compared with their traditional counterparts, such as enhanced catalytic performance,[1] increased sensitivity as sensors,[2] improved mechanical properties,[3] and so on. Particularly, when the feature size (at least 1D) is further confined within mere 1 nm, it is discovered that ultrathin nanocrystals could exhibit extraordinary properties which are even absent in ordinary nanomaterials. Very recently, our group has found that ultrathin GdOOH nanowires with the diameter of 1 nm showed high flexibility analogue to polymer,[4] and ultrathin In_2S_3 nanobelts with the thickness of 1 nm could self-adjust their conformations like biology macromolecules to assemble to highly regular 3D supercrystal.[5] It is believed that such ultrathin nanomaterials could build up a bridge between the inorganic world (inorganic nanocrystals) and the organic world (macromolecules) to establish more significant subjects in the field of nanoscience. However, the exploration of ultrathin nanomaterials is still limited, more ultrathin structures are first required to enrich the research objects for paving the way to develop such materials in nanotechnology.

Nowadays, tremendous efforts have been made to develop the synthetic strategy for nanomaterials under the encouragement of constructing novel nanostructures. For the synthesis of ultrathin nanocrystals through bottom-up route, the key point stands in the confinement of the nuclei formed in early stage within the size of ultrathin range. Within the wet chemistry synthetic system, we found that the combination of good solvent and poor solvent of the ligand-encapsulated clusters could effectively meet the requirement. The introduction of poor solvent could increase the supersaturation of precursors, resulting in the formation of tiny nuclei and followed by ultrathin nanocrystals. When long chain fatty acids/amines are utilized as ligands, combined nonpolar solvent (good solvent) and polar solvent (poor solvent) have been demonstrated to be able to fabricate ultrathin nanocrystals including rare earth hydroxide nanowires,[4] metal oxide nanobelts,[6] and transition metal sulfides superlattices of nanosheets.[7] And there still remains much space to investigate this system for the synthesis of ultrathin nanocrystals.

Nickel molybdate is a kind of excellent electrochemical catalysts. And various 1D nickel molybdate nanostrcutures have been synthesized and utilized as the materials of supercapacitors[8] and lithium battaries.[9] However, to our knowledge, the successful fabrication of ultrathin nickel molybdate nanowires with the diameter down to sub-1 nm has not been reported and the application for water oxidation is also not as blooming as the above two ones. Here in this paper, highly uniform sub-1 nm nickel molybdate nanowires are synthesized through a good/poor solvents system, and the growth process is systematically traced to reveal the growth mechanism behind. The addition of the new example can absolutely enrich and inspire the field of ultrathin nanomaterials. It is found that the ultrathin nanowires can be assembled to macroscopic paper with flexibility owing to the instinct flexibility of the nanowires which may enrich the potential applications of such materials. The activity of the nanowires for oxygen evolution reaction is also evaluated.

The sub-1 nm nickel molybdate nanowires were synthesized by utilizing oleic acid (OA) and oleyamine (OAm) as the combined surfactants. The Fourier transformation infrared (FT-IR) spectrum of the washed products given in Figure S1 (Supporting Information) clearly shows the strong stretching vibrations of CH_3 at 2921 and 2848 cm^{-1} and CH_2 scissor vibration at 1461 cm^{-1} which all derive from the long fatty chains, indicating that the nanowires surface are capped with the introduced surfactants. **Figure 1**a–c exhibit the typical transmission electron microscopy (TEM) images of the ultrathin nanowires. From the overview image in Figure 1a, the nanocrystals seem to be paralleled along "nanobelts" on the copper grid with extremely high purity. However, the "nanobelts" are proved to be neatly aligned nanowires with a uniform diameter of sub-1 nm by the TEM image at high magnification in Figure 1b. The nanowires align side-by-side to contact with a high area under the driven force of decreasing surface energy as the solvent evaporating from the copper grid. The regular arrangement is further confirmed by the high-angle annular dark field scanning transmission electron microscopy (HAADF-STEM) image in Figure 1c

H. Liu, H. Li, P. He, Prof. X. Wang
Department of Chemistry
Tsinghua University
Beijing 100084, China
E-mail: wangxun@mail.tsinghua.edu.cn

DOI: 10.1002/smll.201503150

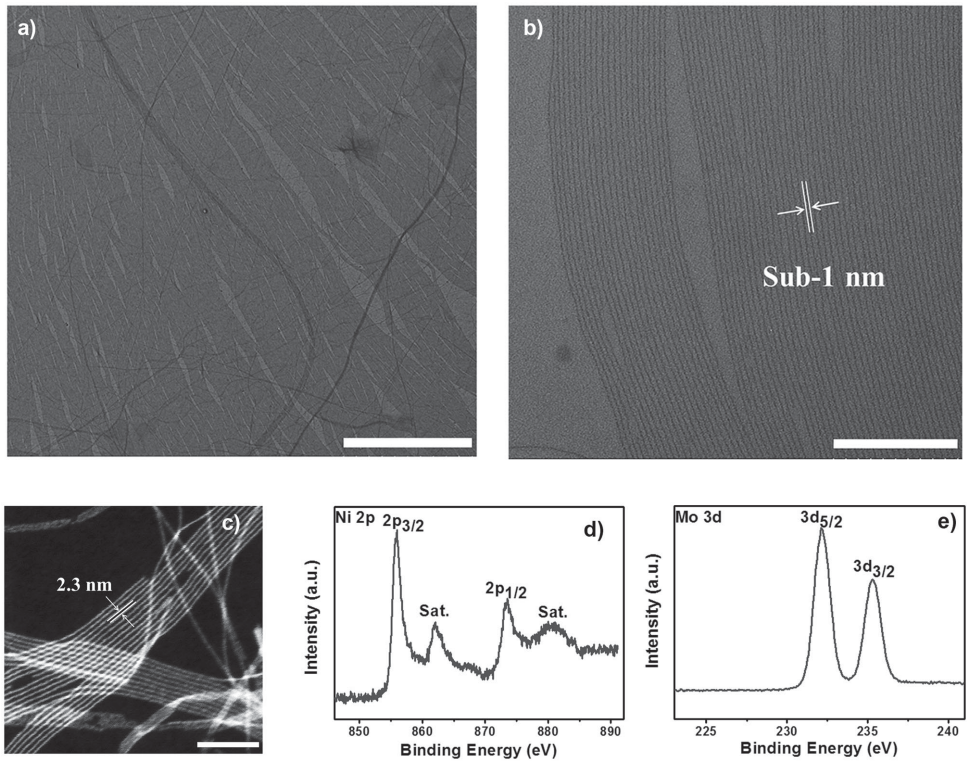

Figure 1. a) Typical low-magnification TEM image and b) high-magnification TEM image of the ultrathin nanowires with high purity. c) STEM image of the well-aligned nanowires. XPS results, d) Ni 2p core level spectrum and e) Mo 3d core level spectrum of the nickel molybdate nanowires. Scale bar: (a) 2 μm; (b) 100 nm; (c) 50 nm.

which exhibits a periodic interval distance of 2.3 nm between nanowires.

To determine the chemical composition of the ultrathin nanowires, a series of examinations including energy dispersive X-ray (EDX), X-ray photo electron spectrum (XPS), and X-ray diffraction (XRD) were conducted on the well washed products. EDX result given in Figure S2 (Supporting Information) confirms that the element ratio between Ni and Mo is 1:1. Inductively coupled plasma mass spectrometry was futher analyzed and gives the ratio to be 1.3. The valence states of the two metals were further analyzed through the XPS results in Figure 1d,e, displaying Ni 2p and Mo 3d levels. The Ni 2p core level spectrum (Figure 1d) is deconvoluted into four peaks. Two peaks at 855.9 and 873.4 eV are indexed to Ni $2p_{3/2}$ and Ni $2p_{1/2}$, respectively, and the doublet separation enhancement up to 17.5 eV indicates the signature of the Ni^{2+} oxide state.[10] Moreover, the other two satellite peaks at 862.1 and 880.7 eV are obviously strong. For Mo 3d level, the spectrum (Figure 1e) exhibits two peaks with binding energies of 232.1 and 235.3 eV, corresponding to Mo $3d_{5/2}$ and Mo $3d_{3/2}$ with the doublet separation of 3.2 eV which signifies a Mo^{6+} oxide state.[11] The peaks in XRD pattern shown in Figure S3 (Supporting Information) are broadened due to the ultrathin feature of the nanowires, making it difficult to be indexed. While considering the analyzed EDX and XPS characterizations combined with the utilized precursors ($NiCl_2{\cdot}6H_2O$, Na_2MoO_4), the XRD pattern is carefully indexed to $NiMoO_4{\cdot}xH_2O$ (JCPDS card 13–0128).

To investigate the growth process of the ultrathin nanowires, a series of samples obtained at various stages of the reaction were monitored. We found that the nanowires growth at the temperature of 140 °C required only 30 min, proved by the appearance of a large amount of long nanowires shown in Figure S4 (Supporting Information). Thus the monitored reaction temperature was decreased to 100 °C to slow down the growth rate for the study of intermediates. Under this temperature at 10 min, the main products are ultrathin nanobelts, coexisting with a small amount of short nanowires. The length of the nanobelts is ≈130 nm and the lateral size of the nanobelts is quite thin indicated by the low contrast under TEM observation in **Figure 2**a. Our group has successfully synthesized a series of ultrathin nanostructures based on good/poor solvents systems. In this case with the similar synthetic conditions, the combined surfactants considered as the good solvent and ethanol as the poor solvent are also believed to endow the ultrathin feature to the nanobelts. Then XPS characterization was further conducted on the early-stage formed nanobelts and the signals of Mo^{6+} were observed without the signals of Ni as shown in Figure S5 (Supporting Information), indicating that the nanobelts contain Mo while no Ni element exists. While the peaks are weak which is probably attributed to the thick capped surfactants, the bonding energies occupy the similar positions with those of the analyzed final products. From the result, we assume that the nanobelts might be the assembly of oxomolybdate clusters confined by surfactants. As the reaction time increases, the nuclei may be induced by the entrance of Ni^{2+} and subsequently formed nickel molybdate component. From 30 min to 6 h, the main products are transformed from nanobelts to sub-1 nm nanowires (Figure S6, Supporting Information). A

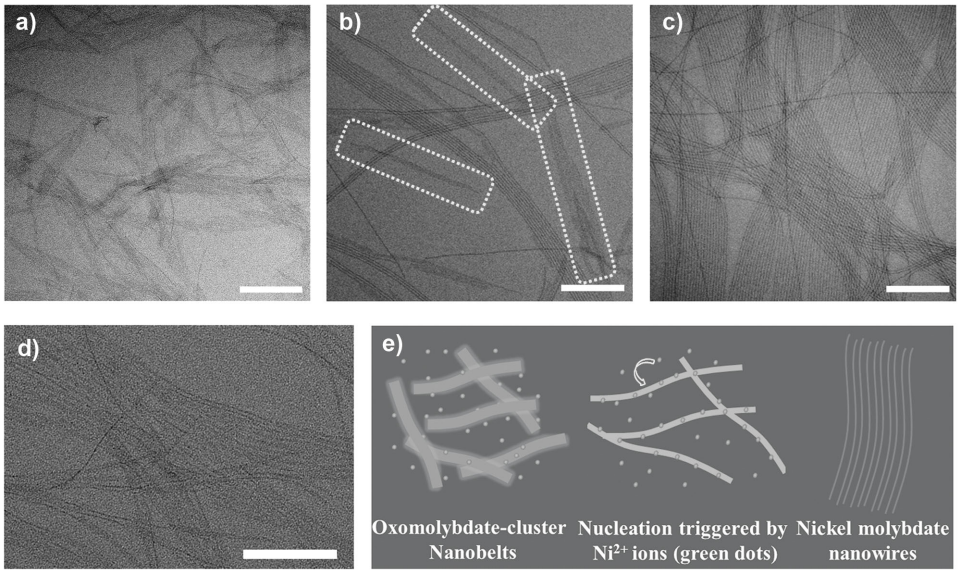

Figure 2. TEM images of the nanowires synthesized at 100 °C for a) 10 min, b) 2 h, c) 12 h, indicating the transformation from more nanobelts to nanowires. d) TEM image of fast-cooling sample heated at 140 °C for 10 min. e) Schematic illustration of the formation of nickel molybdate nanowires. (green dots, Ni^{2+} ions) Scale bar: (a), (b), (c), and (d) is 100 nm.

typical image of the products at reaction time of 2 h shows the formation of nanowires with less remained oxomolybdate-cluster nanobelts marked in Figure 2b. The 1D and ultrathin features of the nanobelts are, to some extent, supposed to template the formation of $NiMoO_4{\cdot}xH_2O$ nanowires with sub-1 nm. This is further confirmed by the products obtained through immediately cooling the autoclave (using flowing water) kept at 140 °C for 10 min. The TEM image in Figure 2d clearly shows the existence of long thin nanobelts with partly in situ formed nanowires. On another aspect, although the crystalline structures of $NiMoO_4{\cdot}xH_2O$ is still unknown, many literatures have reported the construction of 1D $NiMoO_4{\cdot}x$H2O nanostructures.[12] Thus it is assumed that the nickel molybdate might possess 1D chain structure like many other molybdates,[13] also contributing the 1D growth to the nanowires. After 12 h, highly pure nanowires without nanobelts are obtained (Figure 2c). The whole growth process illustrated in Figure 2e is divided into three steps: (1) thin assembled oxomolybdate-cluster nanobelts are formed; (2) Ni^{2+} enters the nanobelts to induce the nuclei; (3) the nanobelts template the following growth.

The influence of the ratio of OA/OAm, reaction temperature and time on the formation of the nanowires is also investigated. It is found that the 2:1 ratio of OA/OAm is the optimal value, more OA leads to the generation of tiny nanoparticles (Figure S7b, Supporting Information), while more OAm tends to give nanosheets (Figure S7a, Supporting Information). The combined surfactants may synergistically confine the nanobelts template and the following growth. However, the growth is not sensitive to the reaction temperature. A wide range from 100 to 210 °C can generate the nanowires with the same sub-1 nm diameter and microlevel length (Figure S8, Supporting Information), indicating the well confined nanowires surface in this system. The difference exists in the formation time, higher temperature results in shorter growth period. What should be paid attention to is that the ultrathin nanowires can be broken into tiny nanoparticles and further grow to large size rods (Figure S9a, Supporting Information) at 210 °C for 1h due to the instability of the nanowires under such high energy input.

Nanowires, as 1D nanomaterials, have exhibited unique optical,[14] electric,[15] and magnetic[16] properties compared with the nanocrystals owning other morphologies. Especially for the nanowires with high aspect ratio, the ideal structure for directing the conduction of electrons, photons, and phonons can further enhance the mentioned properties. Moreover, the high aspect ratio is vital to nanowire macroscopic-scale assembly which is of great significance to promote their real application.[17] Here in our case, the aspect ratio of the nanowires with a diameter of sub-1 nm and length up to micrometer level readily reaches the magnitude of 10^3, enabling the nanowires spontaneously form paper-like film through vacuum filtration procedure. The macroscopic film together with the detailed inner architecture and the mechanical property is highlighted in **Figure 3**. The as-prepared nanowires were first well dispersed in a good solvent, 10 mL cyclohexane, forming a homogeneous solution with the concentration of 0.0055 g cm^{-3}. Then it was mixed with ethanol in an equal volume to cyclohexane and poured through a piece of filter paper under vacuum to construct a film shown in Figure 3a. The size of the film is confined by the size of the filtration funnel and the thickness is dependent on the concentration of the nanowires. The film could be rolled easily as exhibited in Figure 3b, indicating the desirable flexibility which mainly derives from the intrinsic flexible feature of the ultrathin nanowires. Thin film also shows the transparency to some extent in the inset in Figure 3b. Remarkably, the inner structure of the film further characterized by scanning electron microscopy (SEM) is confirmed to be a hierarchical construction. From an overview image given in Figure 3c, the film consists of numerous nanowire bundles that intertwist with each other, resulting in porous framework (Figure 3d).

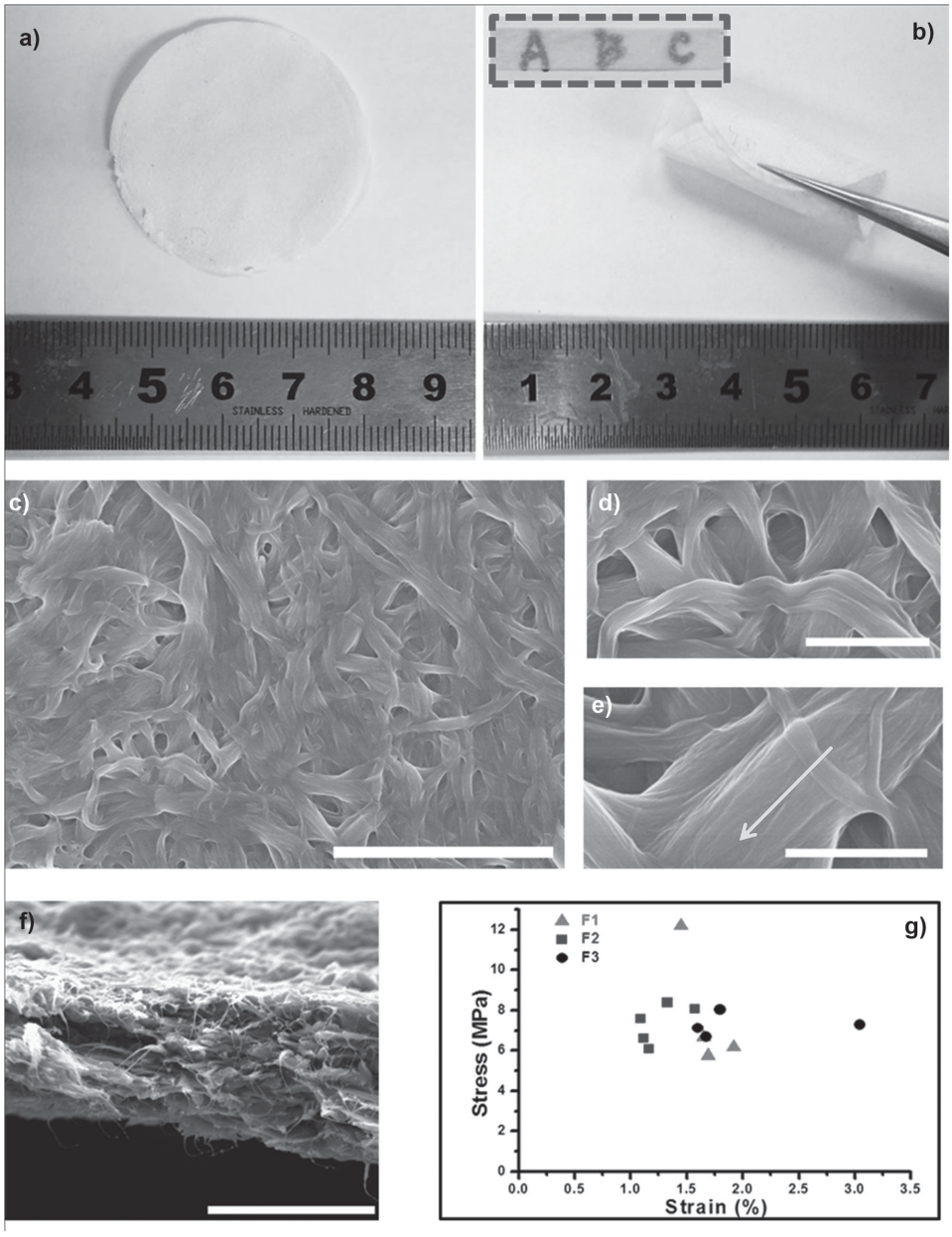

Figure 3. Photographs of a) as-prepared film with the diameter of 3.7 cm, and b) scrolled film which demonstrates the flexibility feature. The inset in (b) shows the clear letters through the transparent film. SEM images of c) nanowires film containing intertwisted bundles, d) formed pores in the film, and e) a selected bundle with the texture resulting from the assembled nanowires. f) SEM image of a typical fracture surface. Scale bar: (c) 20 μm; (d) 2 μm; (e) 1 μm; (f) 20 μm. g) The mechanical properties of three parallel series of standard samples.

A closer examination of a single bundle in Figure 3e shows a parallel texture inside which well dispersed nanowires assemble side-by-side to decrease the surface energy with the addition of ethanol. Different from the films directly stacked by nanowires,[18] a hierarchical structure with the nanowires as primary building blocks and the bundles as secondary units is demonstrated in our case. The mechanical property of the film was quantitatively characterized through testing the fracture stress and strain of a series of films. Based on the results given in Figure 3g, the calculated data are relatively stable except two points. Then the average fracture stress and strain are computed to 6.95 MPa and 1.57%, giving a modulus of 442.7 MPa. Figure 3f shows a typical fracture surface of a tested sample. Despite the demonstrated hierarchical structure of the film, the surfactants capped on the nanowires surface resulting in Van der Waals force between nanowires further contribute the desirable mechanical property. The thermogravimetry analysis (TGA) in Figure S10 (Supporting Information) confirms an approximate 35% fraction of organic surfactants of the film. The scalable formation of film through vacuum filtration due to the extremely high aspect ratio of the nanowires and its flexible feature intrinsically from the ultrathin diameter are believed to be necessary for the large scale application of the materials in the future.

Ultrathin nanocrystals have exhibited their extraordinary advantages as catalysts in a wide range of applications

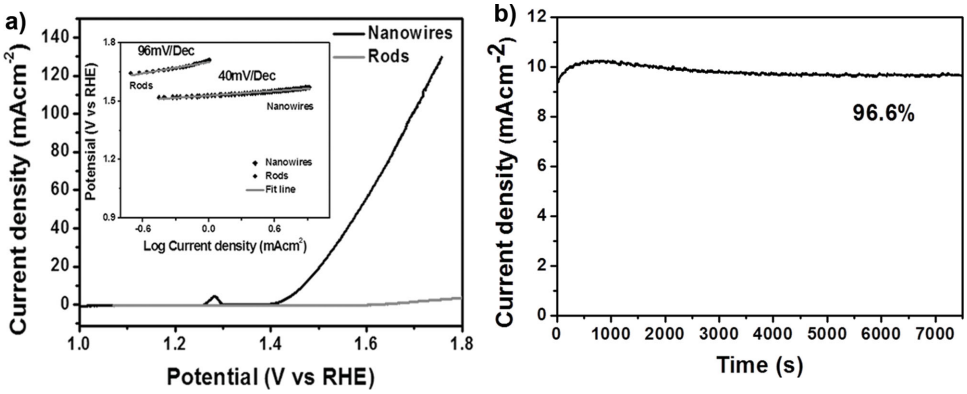

Figure 4. a) Polarization curves of ultrathin nanowires and large sized rods catalysts in O_2-saturated 1 M KOH at a scan rate of 10 mV s^{-1}. The inset is the Tafel plots of the compared samples. b) Potentiostatic test at 1.56 V (RHE), indicating the excellent stability of the nanowires.

due to their novel electron structures, large specific surface area, high exposure of active defects, and so on.[19] While nickel molybdate based nanocrystals as the electrochemical catalysts for oxygen evolution reaction (OER) have been reported recently,[20] the ultrathin counterparts have yet not been investigated. Here, we evaluated the OER performance of the sub-1 nm nickel molybdate nanowires in 1 M KOH aqueous and compared the results with those of the large size rods obtained at 210 °C for 1 h. For an OER catalyst, one of the benchmarks is considered as the operating potential required to achieve a current density of 10 mA cm^{-2} which is approximately the value for a 10% efficient solar-to-fuel conversion device.[21] From the linear scan voltammograms (LSV) given in **Figure 4**a, the benchmark potential of the ultrathin nanowires converted to a reversible hydrogen electrode (RHE) is calculated to 1.56 V, confirming a 330 mV overpotential (η) which is even comparable with the values of IrO_2-based nanomaterials in both alkaline (370 mV)[22] and acid (370 mV)[23] environments. However, for the large size rods, the current density just cannot reach 10 mA·cm^2 even under the operating potential of 1.8 V (overpotential η is 570 mV), indicating a much lower activity of the rods for water splitting compared with the ultrathin nanowires. What's more, the onset potential of ultrathin nanowires is confirmed to be ≈1.41 V which is also much lower than 1.62 V of the rods. And under the potential of 1.62 V for nanowires, the current density reaches as high as 62 mA cm^{-2}. Besides, the tafel slopes of the nanowires and rods, as another key parameter to make an evaluation of OER catalysts, are also measured and compared in the inset in Figure 4a. The slope of nanowires is confirmed to be 40 mV dec^{-1} which is smaller than 96 mV dec^{-1} of rods further suggesting the faster kinetic OER process and higher electrocatalytic activity of the ultrathin nanowires. Electric double-layer capacitance (EDLC, C_{dl}) is measured to further compare the electrochemical active surface area of these two materials. As shown in Figure S11 (Supporting Information), a large electrochemical active surface area of 15.68 mF cm^{-2} possessed by the ultrathin nanowires is confirmed which is 3 magnitudes higher than that of rods. The larger value means higher absorbed reactants on the electrochemical catalyst surface, contributing to both lower overpotential and faster kinetic reaction process for the nanowires. The demonstrated promising electrocatalytic performance of the ultrathin nickel molybdate nanowires may first attribute to their low crystallization combined with ultrathin feature, contributing a high level of structural disorder which usually brings catalytic active sites. Moreover, the large surface area resulted from the sub-1 nm diameter further extends the exposure of active sites and provide a large contact between the electrode materials and electrolytes. Besides, the high aspect ratio of the nanowires is suggested to facilitate the conduction of electrons which is significant for electrochemical reactions. The comparison of the electrochemical impedance spectroscopy analysis between the nanowires and rods is displayed in Figure S12 (Supporting Information). The nickel molybdate nanowires also exhibit excellent stability through the potentiostatic test shown in Figure 4b. After operating at 1.56 V (RHE) for 2 h, the current density ≈10 mA cm^2 can still maintain 96.6%.

In summary, sub-1 nm nickel molybdate nanowires with the length of microscale are successfully synthesized based on a supposed template-directed growth in a good/poor solvents system. The confinement of the early-stage formed intermediate is great essential to construct ultrathin nanocrystals. The strategy developed here is believed can be extended to synthesize other ultrathin nanomaterials. The ultrathin feature combined with the high aspect ratio of the nanowires, on one hand, makes them easy to be assembled to flexible film with hierarchical structure and related mechanical property; on the other hand, results in desirable OER activity and stability. The ultrathin nanowires not only exhibit the potential applications for the fabrication of electrochemical device in the future but also provide a research object for the field of ultrathin nanomaterials.

Experimental Section

Synthesis of Sub-1 nm $NiMoO_4 \cdot xH_2O$ Nanowire: In a typical synthesis, 6 mL ethanol was mixed with the mixture of 1.62 g OAm and 0.89 g OA in a 10 mL-Teflon autoclave to form a homogeneous solution. Then with vigorous stirring, 0.3 mL $NiCl_2$ aqueous solution (10 M) and 0.3 mL Na_2MoO_4 aqueous solution (10 M) was added into the autoclave in sequence. After 10 min, the autoclave was sealed and heated at 140 °C for 4 h. After cooling down to ≈30 °C, the product at the bottom of the autoclave was dispersed

small NANO MICRO

in 10 mL cyclohexane, and then precipitated with the addition of 20 mL ethanol and centrifugated at 8000 rpm for 5 min to remove the excess surfactants. After three cycles of dispersion and centrifugation wash, the green product was dispersed in cyclohexane.

Characterization: The morphologies of the products were observed by using a Hitachi H-7700 transmission electron microscope (TEM) operating at 100 kV and Techai G2 F20 S-Twin high-resolution TEM at 200 kV equipped with high angle annular dark field scanning TEM. The structures of the films were investigated under a field-emission scanning electron microscope (FESEM, Gemini LEO 1530). FTIR spectra were recorded with a Nicolet 205 FTIR spectrometer using the KBr pellet technique. The ratio between Ni and Mo was analyzed by the energy-dispersive X-ray spectroscope attached to the TEM instrument. The XPS test was operated on a VG ESCALAB 200R spectrometer using monochromatic Al Ka radiation. XRD characterization was carried on a Bruker D8 Advance X-ray diffractometer using Cu Kα radiation ($\lambda = 1.5418$ Å). Mechanical property tests were conducted on an Instron 3342 universal testing machine (Instron, USA).

Film Preparation by Vacuum-Filtration and the Mechanical Property Measurement: The ultrathin nanowires were first well dispersed in cyclohexane and then mixed with the equal volume of ethanol to cyclohexane. After sonication for 2 min, fiber-like precipitates appeared and were poured through a piece of filter paper under vacuum, forming a green film on the paper spontaneously. The film could be easily peeled off. To test the mechanical property of the film, three films fabricated with a same amount of nanowires were cut into three series of standard rectangle samples with the length of 30 mm and width of 5 mm. The samples were all tests at a loading rate of 0.5 mm per min. After tests, the sizes of the fractured points were determined by SEM.

Oxygen Evolution Reaction (OER) Electrocatalytic Electrode Preparation and Test: Well-washed product (five wash cycles) fabricated in a 10 mL-Teflon autoclave (≈50 mg) was dispersed in 10 mL toluene. 0.95 mL nanowires dispersion was removed and mixed with 0.05 mL nafion under sonication to form a homogeneous emulsion. Then 6 µL emulsion (≈30 µg) was dropped on the glassy carbon electrode with a surface area of 0.196 cm^2. The mass load was further carefully determined by calculating the concentration of the toluene dispersion by drying the left product and weighted the product. As reported previously by our group, the method of the OER catalyst preparation greatly influenced the final electrochemical test result. When the samples were totally dried and used for the OER as in many other reports, the poor dispensability in both polar solvent (ethanol) and nonpolar solvent (toluene, cyclohexane) gave the samples a much worse electrocatalytic performance.

All the electrochemical tests were operated in O_2 presaturated 1 M KOH electrolyte on a Princeton P4000 electrochemical workstation, utilizing a normal three-electrode cell in which Pt foil and Hg/Hg_2Cl_2 acted as the counter electrode and reference electrode, respectively. Cyclic voltammetry (CV) was first conducted on the electrodes at scan range from –0.2 to 0.5 V and scan rate of 50 mV s^{-1} to stabilize the sample. After 200 CV cycles, linear sweep voltammetry (LSV) at scan rate of 10 mV s^{-1} was measured as the rotation speed of the electrode was set at 1600 rpm. Then, tafel slopes were obtained based on the tafel function of Princeton P4000. The electrocatalytic stability of the nanowires was valued by potentiostatic test, the potential was fixed at 1.56 V (RHE) which was the required value for the generation of 10 mA cm^{-2} current density. The electric double capacitance test was conducted by measuring the CVs in a non-Faradaic region (for nanowires from 0.28 to 0.33 mV, for rods from 0.48 to 0.53 mV) of the voltammogram at following scan rate: 4, 8, 12, 16, 20, and 24 mV s^{-1}. Charging current density measured at 0.305 V versus SCE for nanowires and 0.505 V versus SCE for rods were plotted as a function of scan rate, respectively. The capacitance of the compared materials was confirmed from the value of the slope of the linear fits to the data.

Supporting Information

Supporting Information is available from the Wiley Online Library or from the author.

Acknowledgements

This work was supported by NSFC (21431003, 91127040, 21221062), and the State Key Project of Fundamental Research for Nanoscience and Nanotechnology (2011CB932402).

[1] a) S. Hu, X. Wang, *Chem. Soc. Rev.* **2013**, *42*, 5577; b) F. Saleem, Z. Zhang, B. Xu, X. Xu, P. He, X. Wang, *J. Am. Chem. Soc.* **2013**, *135*, 18304; c) Y. Liu, C. Xiao, M. Lyu, Y. Lin, W. Cai, P. Huang, W. Tong, Y. Zou, Y. Xie, *Angew. Chem. Int. Ed.* **2015**, *127*, 11383; d) L. Liang, H. Cheng, F. Lei, J. Han, S. Gao, C. Wang, Y. Sun, S. Qamar, S. Wei, Y. Xie, *Angew. Chem. Int. Ed.* **2015**, *54*, 12004.
[2] Y. Cui, Q. Wei, H. Park, C. M. Lieber, *Science* **2001**, *293*, 1289.
[3] J. Xu, H. Wang, C. Liu, Y. Yang, T. Chen, Y. Wang, F. Wang, X. Liu, B. Xing, H. Chen, *J. Am. Chem. Soc.* **2010**, *132*, 11920.
[4] S. Hu, H. Liu, P. Wang, X. Wang, *J. Am. Chem. Soc.* **2013**, *135*, 11115.
[5] P.-P. Wang, Y. Yang, J. Zhuang, X. Wang, *J. Am. Chem. Soc.* **2013**, *135*, 6834.
[6] J. He, H. Liu, B. Xu, X. Wang, *Small* **2015**, *11*, 1144.
[7] P. P. Wang, H. Sun, Y. Ji, W. Li, X. Wang, *Adv. Mater.* **2014**, *26*, 964.
[8] D. Guo, P. Zhang, H. Zhang, X. Yu, J. Zhu, Q. Li, T. Wang, *J. Mater. Chem. A* **2013**, *1*, 9024.
[9] J. Haetge, I. Djerdj, T. Brezesinski, *Chem. Commun.* **2012**, *48*, 6726.
[10] J. Yan, Z. Fan, W. Sun, G. Ning, T. Wei, Q. Zhang, R. Zhang, L. Zhi, F. Wei, *Adv. Funct. Mater.* **2012**, *22*, 2632.
[11] X. Xia, W. Lei, Q. Hao, W. Wang, X. Wang, *Electrochim. Acta* **2013**, *99*, 253.
[12] D. Ghosh, S. Giri, C. K. Das, *Nanoscale* **2013**, *5*, 10428.
[13] a) K. Saito, S. Kazama, K. Matsubara, T. Yui, M. Yagi, *Inorg. Chem.* **2013**, *52*, 8297; b) Z. A. Solodovnikova, S. F. Solodovnikov, *Acta Crystallogr., Sect. C* **2006**, *62*, 53.
[14] a) M. H. Huang, S. Mao, H. Feick, H. Yan, Y. Wu, H. Kind, E. Weber, R. Russo, P. Yang, *Science* **2001**, *292*, 1897; b) X. Liu, L. He, J. Zheng, J. Guo, F. Bi, X. Ma, K. Zhao, Y. Liu, R. Song, Z. Tang, *Adv. Mater.* **2015**, *27*, 3273.
[15] J. Hu, M. Ouyang, P. Yang, C. M. Lieber, *Nature* **1999**, *399*, 48.
[16] R. Skomski, H. Zeng, M. Zheng, D. J. Sellmyer, *Phys. Rev. B* **2000**, *62*, 3900.

[17] a) X. Zhang, T. Zhang, J. Ng, D. D. Sun, *Adv. Funct. Mater.* **2009**, *19*, 3731; b) X. Peng, J. Jin, E. M. Ericsson, I. Ichinose, *J. Am. Chem. Soc.* **2007**, *129*, 8625.
[18] a) X. Qi, F. E. Osterloh, J. Giacomo, S. Chiang, *Langmuir* **2006**, *22*, 8253; b) J. Yuan, X. Liu, O. Akbulut, J. Hu, S. L. Suib, J. Kong, F. Stellacci, *Nat. Nanotechnol.* **2008**, *3*, 332.
[19] H. Yin, S. Zhao, K. Zhao, A. Muqsit, H. Tang, L. Chang, H. Zhao, Y. Gao, Z. Tang, *Nat. Commun.* **2015**, DOI: 10.1038/ncomms7430.
[20] R. Singh, R. Awasthi, A. Sinha, *J. Solid State Electrochem.* **2009**, *13*, 1613.
[21] C. C. McCrory, S. Jung, J. C. Peters, T. F. Jaramillo, *J. Am. Chem. Soc.* **2013**, *135*, 16977.
[22] Y. Zhao, R. Nakamura, K. Kamiya, S. Nakanishi, K. Hashimoto, *Nat. Commun.* **2013**, *4*, 2390.
[23] W. Hu, Y. Wang, X. Hu, Y. Zhou, S. Chen, *J. Mater. Chem.* **2012**, *22*, 6010.

Received: October 17, 2015
Revised: November 18, 2015
Published online: January 3, 2016